

NBAvatar: Neural Billboards Avatars with Realistic Hand-Face Interaction

David Svitov^{1,2} and Mahtab Dahaghin^{1,2}

¹ Università degli Studi di Genova, Italy

² Istituto Italiano di Tecnologia (IIT) Genova, Italy
{david.svitov,mahtab.dahaghin}@iit.it

Abstract. We present NBAvatar - a method for realistic rendering of head avatars handling non-rigid deformations caused by hand-face interaction. We introduce a novel representation for animated avatars by combining the training of oriented planar primitives with neural rendering. Such a combination of explicit and implicit representations enables NBAvatar to handle temporally and pose-consistent geometry, along with fine-grained appearance details provided by the neural rendering technique. In our experiments, we demonstrate that NBAvatar implicitly learns color transformations caused by face-hand interactions and surpasses existing approaches in terms of novel-view and novel-pose rendering quality. Specifically, NBAvatar achieves up to 30% LPIPS reduction under high-resolution megapixel rendering compared to Gaussian-based avatar methods, while also improving PSNR and SSIM, and achieves higher structural similarity compared to the state-of-the-art hand-face interaction method InteractAvatar.

Project page: david-svitov.github.io/NBAvatar_project_page.

Keywords: Face Interaction · Neural Rendering · Gaussian Splatting

1 Introduction

The interaction between hands and face is an important source of information in human communication [12, 33] and therefore is of paramount importance for telepresence and virtual reality applications. Such applications rely on rendering of the dynamic hand and face, but struggle to realistically represent their interaction. Modern methods concentrate solely on head [13, 15, 16, 30, 40, 46, 62, 64] or hand [9, 11, 19, 20, 23, 36, 38] rendering and leave their mutual interaction out of scope. While a few methods [8, 21] attempt to handle the rendering of hand-face interaction, they often struggle with artifacts that limit their applicability. In this work, we address the task of photo-realistically rendering of face-hand interactions (Fig. 1 (a)), accounting for non-rigid face deformation and color changes under both novel viewpoints and novel poses - the latter being essential for avatar animation and self and cross-reenactment (Fig. 1 (b)) in telepresence.

Head avatar methods [16, 40, 46, 54, 64] rely on different rendering approaches to achieve photo-realistic novel-view synthesis. NeRF-based methods [15, 17, 26,

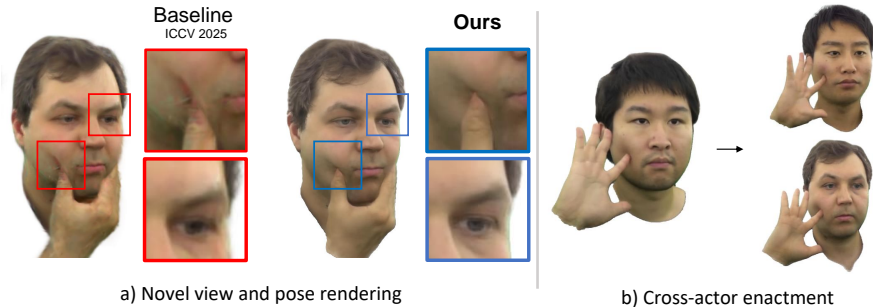


Fig. 1: Novel view synthesis. We present the method for photo-realistic novel-view rendering of non-rigid hand-face interaction scenarios for human avatars. a) Our method achieves photo-realistic rendering quality for novel views and poses, surpassing state-of-the-art InteractAvatar [8] results. b) The method enables cross-actor enactment by transferring hand and face poses across different subjects.

[31, 64] provide view-consistent rendering but suffer from slow inference, even with acceleration techniques [35, 64]. DNR [54] achieves real-time speed by deferring neural processing to screen space, but tends to produce view-dependent overfitting artifacts due to limited underlying mesh detail. The breakthrough in human avatar representation happened with the appearance of 3D Gaussian Splatting (3DGS) [24]. Modern head avatar methods [28, 40, 45, 46] utilize 3DGS to handle realistic animated rendering [40, 46] and lighting effects [28, 45]. While the head avatar’s rendering quality has significantly improved, non-rigid face deformations and hand-face interactions remain underrepresented. Pioneering approaches [21, 47, 58] in hand-face interaction aimed to predict face mesh deformation caused by hand touch, but did not target rendering realism. Decaf [47] first solved the task of predicting face mesh non-rigid deformations by introducing an encoder-decoder model to predict hand-face interaction area and mesh offsets from monocular video. The pipeline proposed in [21] is among the first to render the resulting mesh using a rendering network, but it produces excessively blurred results. The recent work InteractAvatar [8] represents appearance using 3DGS and interaction-aware MLPs predicting pose-driven color and position offsets. While InteractAvatar successfully simulates self-cast shadows and face deformations, it inherits 3DGS-specific artifacts, blurry facial textures and Gaussians protruding at the body boundary, that limit its realism (Figure 1(a)).

In this work, we propose a novel **Neural Billboard** primitive that represents the scene as a synergy of implicit and explicit learnable representations. Neural Billboards use implicit neural fields encoded with neural textures [54] along the surface of explicit 3D-oriented billboards [52]. While textured billboard primitives [52] offer surface-aligned explicit geometry, their RGB parameterization limits adaptivity in dynamic contact regions. Conversely, neural textures [54] enable view- and pose-dependent effects but were originally designed for fixed mesh parameterizations and are unstable when naively applied to independently

transformable planar primitives. Neural Billboards successfully adapts the neural texture paradigm to learnable planar primitives describing the avatar surface.

Combining neural textures with billboard splatting is a non-trivial task: without additional constraints, the optimization becomes ill-posed as geometry and appearance compete to explain silhouette and shading changes. To ensure convergence of our dual avatar representation, we propose a training technique that disentangles geometry and appearance during optimization by introducing an additional intermediate segmentation optimization. To summarize, our contributions are as follows:

- We introduce Neural Billboards, a hybrid representation that reconciles surface-aligned planar primitives with deferred neural rendering.
- We propose a geometry-aware training scheme with intermediate silhouette supervision that stabilizes joint optimization of spatial and neural texture parameters.
- We demonstrate that implicit spatial feature aggregation in screen space is sufficient to model complex hand-face interaction effects without explicit interaction-conditioned modules.

2 Related Works

Rendering Methods. Deferred Neural Rendering (DNR) [54] for the first time achieved photorealistic avatar rendering by decoupling geometry from appearance: a mesh is rasterized with per-vertex learned neural feature vectors, and the resulting screen-space feature image is decoded into a photorealistic output by a convolutional network. This design enables high visual fidelity at real-time inference speed, since the computationally expensive neural processing is deferred to a single image-space pass rather than applied per-point in 3D [31]. However, the rendering quality remains tied to the resolution and accuracy of the underlying mesh, as the feature maps are defined on mesh vertices.

Neural Radiance Fields (NeRF) [31] represent scenes as continuous volumetric functions evaluated along camera rays, enabling high-quality novel view synthesis but incurring substantial computational cost due to dense MLP evaluation. Subsequent acceleration techniques [7, 14, 35] improved efficiency but retained volumetric ray sampling, limiting real-time performance.

3D Gaussian Splatting (3DGS) [24] reconciled quality and speed by returning to explicit primitives: the scene is represented as a collection of 3D Gaussians that are projected into the image-space, enabling real-time rendering with quality competitive to NeRF. 2D Gaussian Splatting (2DGS) [22] proposed planar Gaussians that align better with object surfaces, improving geometric accuracy and enabling more reliable mesh extraction. To reduce the number of primitives required for fine texture detail, Billboard Splatting (BBSplat) [52] replaces each 2D Gaussian with a textured planar primitive that carries learnable RGB textures and alpha maps.

Head Avatars. To model realistic, drivable head avatars, early mesh-based approaches [3, 4, 37] used parametric 3D Morphable Models (3DMM), such as

FLAME [29], fitted to facial images, but were limited to low-frequency appearance due to coarse per-vertex attributes. Texture-based extensions [13, 16, 30] improved visual fidelity by attaching RGB textures to the mesh surface, yet remained constrained by the fixed resolution and topology of the underlying geometry. DNR [54] proposed to utilize learned neural feature maps instead of hand-crafted textures to represent out-of-mesh details via deferred rendering. Subsequent works [1, 5, 17] further explored neural texture representations for face avatars. While such models enable realistic rendering, they often produce overfitting artifacts on the out-of-mesh details.

The NeRF [31] representation enabled view-consistent realistic rendering and shifted the field toward fully implicit representations. NerFace [15] and IMAvatar [62] conditioned NeRFs on 3DMM parameters to enable controllable synthesis from monocular video, with IMAvatar further improving generalization to unseen expressions through learned implicit blendshapes and skinning fields. However, these methods suffered from prohibitively slow volumetric rendering. INSTA [64] and AvatarMAV [60] partially addressed this by embedding radiance fields within efficient spatial data structures, but the fundamental overhead of volumetric ray sampling remained.

3DGS [24] resolved the speed-quality trade-off by introducing explicit Gaussian primitives to represent the scene. PointAvatar [63] pioneered deformable point-based head avatars from monocular video, while GaussianAvatars [40] and SplattingAvatar [46] established the hybrid mesh-Gaussian paradigm by binding Gaussian kernels to FLAME [29] template mesh surfaces, enabling controllable animation with real-time rendering. More recently, CloseUpAvatar [53] replaced Gaussians with textured billboard primitives [52], achieving high-fidelity rendering across a wider range of camera distances, but assuming a static appearance of avatars. Despite these advances, all of the above methods focus exclusively on head modeling and do not address the dynamics of hand-face interaction.

Hand-Face Interaction. While significant progress has been made in reconstructing photorealistic heads [13, 15, 16, 30, 40, 46, 62, 64] and hands [9, 11, 19, 20, 23, 36, 38] independently, the photo-realistic rendering of the non-rigid deformations and color change caused by hand-face contact remains underrepresented in the literature. One of the first works in the field is Decaf [47], which introduced a monocular RGB method for jointly tracking hand-face interactions and estimating facial deformations using a position-based dynamics (PBD) [34] simulator. DICE [58] extended this to end-to-end estimation via a Transformer architecture. NePHIM [55] proposed a volumetric simulation incorporating temporal effects, anatomical constraints, and skin-pulling dynamics, approximated by lightweight neural networks for real-time performance. However, all of these methods operate solely at the mesh level, without addressing photorealistic rendering. He et al. [21] proposed to learn a PCA basis for hand-induced facial deformations, achieving physically plausible reconstructions, but the focus remains on geometry rather than high-fidelity appearance.

InteractAvatar [8], directly extended the hybrid mesh-Gaussian paradigm [40, 46] to handle realistic rendering of hand-face interactions. While 3DGS-based

approaches produce compelling face reconstructions, they lack mechanisms for pose-dependent appearance dynamics or non-rigid inter-body deformation, resulting in artifact-prone contact regions. InteractAvatar addresses this by augmenting the framework with MLPs to control the appearance of the dynamic hand and interaction region. These MLPs predict offsets on the MANO [42] hand mesh and PBD-initialized facial deformation area based on the hand pose, face expression, and global geometric features calculated by a PointNet++ [39].

While InteractAvatar achieves realistic rendering quality, it remains subject to 3DGS-related artifacts caused by the Gaussians’ displacements. These artifacts are particularly noticeable along the outline of the avatar, resulting in a frosty pattern, as well as general blurriness of the face. Our approach circumvents these issues by combining explicit and implicit representations, such as Billboards [52] and DNR [54] neural textures to handle high-frequency and pose-dependent effects.

3 Method

3.1 Preliminaries: Billboard Splatting

Billboard Splatting was introduced in [52] as a texture-based alternative to 3D Gaussian Splatting (3DGS) [24] and its 2D variant (2DGS) [22]. The method represents a scene using textured surfels (billboards) instead of volumetric Gaussians. Unlike other texture-driven primitives [43, 49, 57, 59], the proposed representation jointly optimizes both RGB and opacity textures while maintaining real-time rendering performance.

The spatial parametrization follows the 2DGS formulation for position and orientation, while augmenting each primitive with learnable texture maps. Specifically, each billboard is defined as $\{\mu_i, s_i, r_i, \text{SH}_i, T_i^{\text{RGB}}, T_i^\alpha\}$, where $\mu_i \in \mathbb{R}^3$ denotes the 3D center, $s_i \in \mathbb{R}^2$ the anisotropic 2D scale, and $r_i \in \mathbb{R}^4$ the quaternion encoding its rotation. The term $\text{SH}_i \in \mathbb{R}^{4 \times 3}$ represents spherical harmonics coefficients, while the values $\{T_i^{\text{RGB}}, T_i^\alpha\}$ correspond to learnable textures of size $S^T \times S^T$ texels for color and opacity.

For rendering, BBSplat employs an explicit ray-splat intersection algorithm [48] to compute billboard-space coordinates (u, v) corresponding to a screen-space pixel (x, y) . The normalized coordinates $(u, v) \in [-1, 1]$ are then mapped to the discrete texture grid and used to sample values from T_i^{RGB} and T_i^α .

3.2 Neural Texture Primitives

In this work, we propose to combine explicit Billboard-based representation [52] with implicit Neural Textures (NT) introduced in DNR [54] as shown in Figure 2. We utilize the explicit representation to describe the avatar’s geometry, while implicit NTs handle view- and pose-dependent color effects. The combination of different representations unlocks drivable avatars with photo-realistic detail and real-time rendering. To this end, we introduce a novel **Neural Billboard** primitive that relies on a learnable billboard’s position and orientation $\{\mu_i, s_i, r_i\}$, but

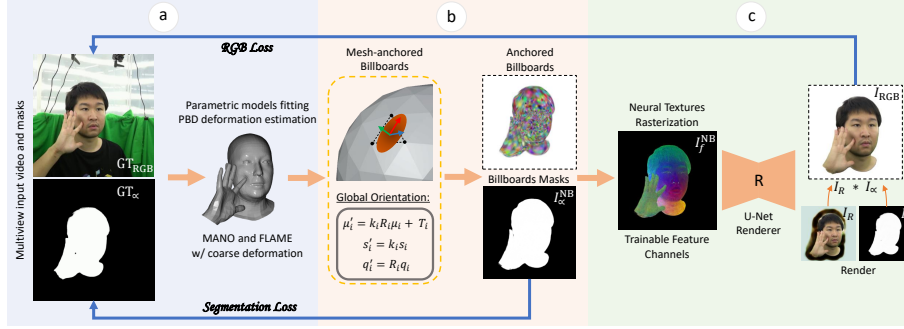


Fig. 2: Method description. a) For multi-view input video, we fit FLAME [29] and MANO [42] parametric models and reconstruct coarse face deformation with position-based dynamics (PBD) [34]. b) Then, for each polygon in the mesh, we anchor Neural Billboards by computing its orientation as offsets relative to the polygon. We rasterize Neural Billboards into a 6-channel image and a corresponding alpha map. c) Finally, we transform this rasterization to RGB with the U-Net renderer R while regularizing the alpha map to fit the ground truth silhouette.

replaces RGB T_i^{RGB} textures with a trainable feature map T_i^{NT} . Thus, the final parametrization of the Neural Billboards is $\{\mu_i, s_i, r_i, T_i^{\text{NT}}, T_i^\alpha\}$. We train our Neural Billboard representation for an avatar in an end-to-end manner where T_i^{NT} and T_i^α are optimized with gradients from the image space losses. While T_i^{NT} learns feature values, T_i^α is responsible for learning visibility of the planar primitives as shown in Figure 3.

During training and inference, each Neural Billboard utilizes neural texture T_i^{NT} with 6 channels. We start by initializing these textures with spectral coordinates following StylePeople [18]. Then we rasterize Neural Billboards into a 6-channel feature map I_f^{NB} and a 1-channel opacity map I_α^{NB} by accumulating neural texture values along the camera rays:

$$c(x) = \sum_{i=1} T_i^{\text{NT}}[\mathbf{u}(x)] T_i^\alpha[\mathbf{u}(x)] \prod_{j=1}^{i-1} (1 - T_j^\alpha[\mathbf{u}(x)]), \quad (1)$$

where \mathbf{u} is UV -coordinates on the billboard that correspond to the screen space point x . The optimization of T_i^α starts with a Gaussian distribution and learns visibility for each planar point \mathbf{u} .

We then employ a UNet-based [44] model to transform a 6-channel rasterization I_f^{NB} into an RGB render I_R as shown in Figure 2 (c). The UNet renderer R produces the final RGB output I_R along with the transparency map I_α , which we combine with background color C_{bg} to obtain the final avatar visualization:

$$I_{\text{RGB}} = I_R I_\alpha + (1 - I_\alpha) C_{bg}. \quad (2)$$

The neural renderer R not only provides high-frequency details but also introduces interaction-aware inductive bias via spatial feature aggregation. Intu-

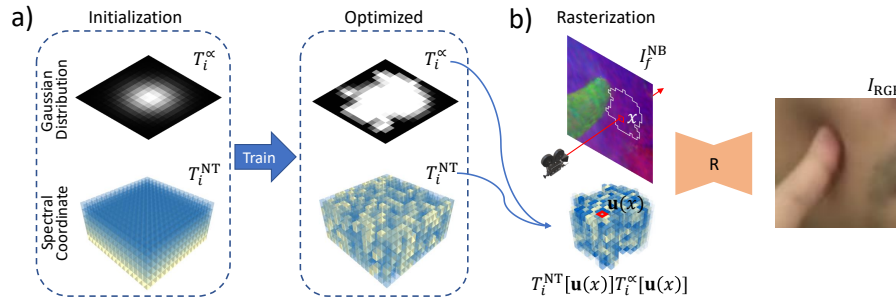


Fig. 3: Neural billboards rasterization. a) We initialize the alpha texture T_i^α with a Gaussian distribution, and fill neural texture T_i^{NT} with corresponding spectral coordinates on the mesh surface. During training, we optimize both textures with gradients from the rasterizer. b) We rasterize screen point x by accumulating corresponding texture values along the ray. The resulting I_f^{NB} transforms to RGB with a trainable renderer R .

tively, the renderer can alter the interpretation of features based on their neighboring values. We deliberately avoid introducing explicit interaction-conditioned modules and rely on spatial feature aggregation in the deferred renderer to implicitly capture contact dynamics. Since both hand and face features are rasterized into a shared screen-space representation, their proximity naturally modulates the decoder’s response within its receptive field. This reduces model complexity and improves generalization to unseen interaction configurations, as the renderer operates purely on spatial feature distributions rather than predefined interaction cues.

We developed a specialized technique to train our Neural Billboard representation that ensures convergence for both billboard orientation and NT features. To disentangle the training of spatial orientation from neural features, we introduce an additional segmentation loss for I_α^{NB} that we discuss in Section 3.4.

3.3 Driving Avatar Animation

First, we fit FLAME [29] and MANO [42] parametric models to the multi-view input video (Fig. 2 (a)) based on the detected facial keypoints and hand joints. We also utilize the off-the-shelf SAM3 [6] model to accurately segment head and hand regions in input frames. We adjusted the SAM3 prompt to capture only areas that can be represented by available parametric models, namely the head and neck and the hand above the wrist. To capture coarse head mesh deformation caused by interaction with the hand, we use position-based dynamics (PBD) [34] physics simulation widely used to model complex skin deformations [2, 10, 50].

As shown in Figure 2 (b), we then adapt a common approach to drive 3DGS-based avatars [8, 40, 51] and anchor Neural Billboards to the mesh surface by calculating their global orientation based on the corresponding i -th polygon transformation $\{T_i, R_i, k_i\}$:

$$\mu'_i = k_i R_i \mu_i + T_i \quad (3)$$

$$s'_i = k_i s_i \quad (4)$$

$$q'_i = R_i q_i \quad (5)$$

Thus, the resulting primitives move along with the parametric mesh surface. Multiplying the billboards’ orientation by the polygon rotation R_i and scale k_i ensures that planar primitives are aligned with the mesh surface in the initial training steps. We also regularize their positions as described in Section 3.4.

3.4 Geometry and Appearance Disentanglement

Unlike mesh-based neural textures, our planar primitives undergo independent rigid transformations during animation. This creates an optimization ambiguity: high-frequency appearance effects can be absorbed either by neural features or by the spatial drift of billboards. To address this, we introduce intermediate silhouette supervision at the billboard rasterization stage, explicitly constraining the geometry before neural decoding. This training scheme is essential for stabilizing the joint optimization of spatial and feature parameters.

To achieve this, we utilize a segmentation loss at the Neural Billboards rasterization stage to ensure that the billboards are tightly fitted to the ground-truth silhouette. This way, we disentangle rigid avatar geometry from view- and pose-dependent appearance, such as shadows from self occlusions or small soft tissue deformations from the hand-face interaction. We optimize Neural Billboard transparency maps I_α^{NB} with Dice [32] segmentation loss:

$$\mathcal{L}_{NB} = \lambda_{NB} \text{Dice}(I_\alpha^{\text{NB}}, \text{GT}_\alpha) \quad (6)$$

The use of billboard segmentation loss is essential to avoid rendering artifacts as shown in the ablation study in Figure 7. Please note that we employ a segmentation loss only to ensure billboard alignment during learning of explicit avatar representations. The renderer segmentation map I_α is optimized implicitly by using random background colors C_{bg} during RGB training. For the final rendering, we use MSE and perceptual LPIPS [61] loss to train an avatar:

$$\mathcal{L}_{RGB} = \|I_{\text{RGB}} - \text{GT}_{\text{RGB}}\|_2^2 + \lambda_{\text{lpiPs}} \mathcal{L}_{\text{lpiPs}} \quad (7)$$

Finally, we apply KNN regularization \mathcal{L}_{KNN} [27, 51] to splatting primitives to constrain the transformations of neighboring billboards and to introduce inductive bias similar to that of convolution neural networks. We push rotation q'_i and scale s'_i for the three nearest billboards to have small standard deviations, while also reducing the distances between them. To improve control over the animation, we also regularize the relative billboard positions μ_i to be close to zero (*i.e.* to the mesh surface). Thus, the final regularization term is as follows:

$$\mathcal{L}_{Reg} = \lambda_{KNN} \mathcal{L}_{KNN} + \lambda_\Delta \mathcal{L}_\Delta \quad (8)$$

Table 1: Novel-view synthesis The metrics reported for megapixel resolution on the Decaf [47] dataset. Best results are in **bold**, second best are underlined. \uparrow : higher is better, \downarrow : lower is better.

Method	S1			S2			S3			S4			Mean		
	PSNR \uparrow	SSIM \uparrow	LPIPS \downarrow	PSNR \uparrow	SSIM \uparrow	LPIPS \downarrow	PSNR \uparrow	SSIM \uparrow	LPIPS \downarrow	PSNR \uparrow	SSIM \uparrow	LPIPS \downarrow	PSNR \uparrow	SSIM \uparrow	LPIPS \downarrow
SA [46]	26.85	0.964	0.059	26.93	0.967	0.057	<u>23.06</u>	0.946	0.094	23.83	<u>0.941</u>	0.109	25.17	0.955	0.080
GA [40]	<u>27.13</u>	0.967	<u>0.054</u>	<u>27.32</u>	<u>0.971</u>	<u>0.053</u>	23.05	<u>0.947</u>	<u>0.091</u>	<u>23.73</u>	0.942	<u>0.106</u>	<u>25.31</u>	<u>0.957</u>	<u>0.076</u>
Ours	27.19	<u>0.966</u>	0.042	28.63	0.976	0.032	23.45	0.951	0.066	23.33	0.940	0.082	25.65	0.958	0.056

4 Experiments

We compared our method against state-of-the-art head avatar approaches GaussianAvatars [40] and SplattingAvatar [46], and state-of-the-art hand-face interaction rendering approach InteractAvatar [8]. We provide quantitative standard objective metrics and qualitative comparisons with baseline approaches on the Decaf [47] hand-face interaction multi-view dataset. In this section, we discuss our choice of baselines and datasets and provide a discussion on the results.

4.1 Implementation

To train the avatar appearance, we set the perceptual loss $\lambda_{l_{lips}} = 0.1$ and applied it to the entire image for the first 40,000 iterations and to random 256×256 crops for the rest of the training to learn fine detail. MSE loss was used throughout training to preserve the subject’s correct colors. We set intermediate segmentation loss coefficients for Billboard segmentation $\lambda_{NB} = 0.1$. For the regularization term, we set $\lambda_{KNN} = 0.1$ and $\lambda_{\Delta} = 0.001$ to ensure billboards alignment along the mesh.

We trained the neural textures and the renderer R end-to-end for 400,000 iterations with a batch size of 1, using the Adam [25] optimizer for all parameters. We used a learning rate of 0.0005 for textures and 0.001 for the renderer, and set the billboards orientation parameters as recommended in [52]. We utilized standard UNet architecture and adapted it for deferred rendering by adding two separate heads for I_{RGB} and I_{α} rendering at 1024×1024 resolution. For training and inference of all subjects we used a single NVIDIA GeForce RTX 4090 GPU.

We use 16×16 textures with six channels for neural texture T_i^{NT} and a single channel for alpha texture T_i^{α} , and anchored a single billboard to each mesh polygon. We adapted StopThePop [41] per-ray sorting of surfel primitives to support neural textures and will open the code of the proposed method to the community. Please refer to the supplementary materials for further implementation details.

4.2 Evaluation Setup

Datasets. We evaluate hand-face interaction on the Decaf [47] dataset, which is the only publicly available dataset providing multi-view video of subjects performing hand-face interactions with calibrated cameras and fitted FLAME

Table 2: Self-reenactment. The metrics reported for megapixel resolution on the Decaf [47] dataset. Avatars are driven by held-out poses from the same subject.

Method	S1			S2			S3			S4			Mean		
	PSNR↑	SSIM↑	LPIPS↓												
SA [46]	<u>28.04</u>	0.974	0.051	24.06	0.946	<u>0.086</u>	<u>26.96</u>	0.974	0.045	<u>24.21</u>	0.954	0.083	25.82	0.962	0.066
GA [40]	27.89	<u>0.974</u>	<u>0.050</u>	<u>21.67</u>	0.933	0.094	26.62	<u>0.975</u>	<u>0.042</u>	24.00	0.957	<u>0.077</u>	25.04	0.960	<u>0.066</u>
Ours	28.45	0.977	0.034	21.62	<u>0.934</u>	0.085	27.20	0.977	0.032	24.66	0.957	0.059	<u>25.48</u>	<u>0.961</u>	0.052

Table 3: Comparison with the metrics reported in the InteractAvatar [8] paper. We reproduced the evaluation pipeline for our method as closely as possible, and InteractAvatar results are taken directly from the original paper.

(a) Novel View				(b) Self-Reenactment			
Method	PSNR↑	SSIM↑	LPIPS↓	Method	PSNR↑	SSIM↑	LPIPS↓
IA [8]	29.85	0.933	0.034	IA [8]	28.17	0.936	0.040
Ours	24.41	0.936	0.051	Ours	24.20	0.942	0.048

and MANO parameters. Following the experiments of InteractAvatar [8], we use four subjects and train on seven views while holding out one view for novel view evaluation. We preprocess data by segmenting head and hand out of the image by using the SAM3 [6] off-the-shelf model, and respectively resize frames to megapixel resolution of 1024×1024 with central crop for our experiments and to a small 512×512 resolution to directly compare with results reported in InteractAvatar [8]. For the last one, we cropped the images using the tracked bounding boxes of the head and hand.

Baselines. We compare NBAvatar against three state-of-the-art methods: GaussianAvatars [40] (GA), which attaches 3D Gaussians to 3DMM mesh triangles; SplattingAvatar [46] (SA), which embeds Gaussians on the mesh surface with learnable migration; and InteractAvatar [8] (IA), which extends the mesh-Gaussian paradigm with interaction-aware MLPs for hand-face deformation and appearance. Both GA and SA are the latest hybrid Gaussian head avatar methods that anchor Gaussians to the head template mesh. We naively extend their representation to model hands driven by the MANO hand template mesh.

Metrics. For quantitative evaluation, following the previous works, we report three standard image quality metrics: Peak Signal-to-Noise Ratio (PSNR), Structural Similarity Index Measure (SSIM) [56], and Learned Perceptual Image Patch Similarity (LPIPS) [61]. While PSNR and SSIM indicate pixel-level reconstruction quality and color matching, LPIPS provides a human perceptual correlated metric.

4.3 Quantitative Results

Table 1 reports the quantitative results for novel-view rendering with megapixel resolution. Our NBAvatar achieves the best average scores across all three met-

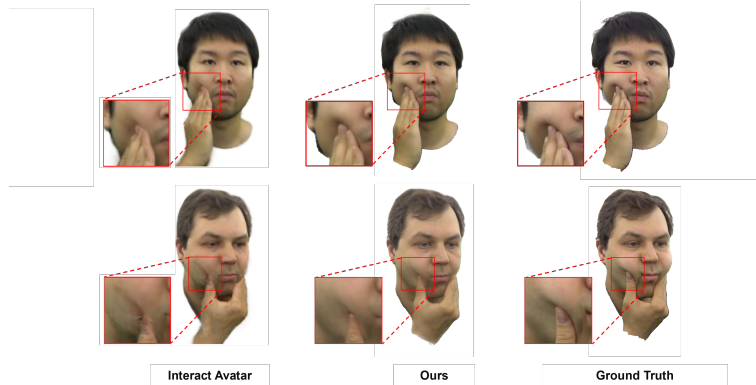


Fig. 4: Qualitative comparison with InteractAvatar [8]. Despite achieving lower PSNR under their evaluation protocol, NBAvatar produces sharper details and more realistic hand-face deformations. InteractAvatar exhibits characteristic 3DGS artifacts including blurry facial textures and protruding Gaussians along the avatar boundary.

rics, with a mean PSNR of 25.65 dB, SSIM of 0.958, and LPIPS of 0.056. Notably, NBAvatar reduces the mean perceptual distance (LPIPS) by 26.3% relative to GaussianAvatars (0.056 vs. 0.076) and by 30.0% relative to SplattingAvatar (0.056 vs. 0.080). The improvement in LPIPS is particularly significant, as it reflects the perceptual quality gains enabled by our Neural Billboard primitives, which capture fine-grained pose-dependent appearance details that pure Gaussian splatting cannot represent.

Table 2 reports the self-reenactment results, where avatars are driven by held-out poses from the same subject to evaluate under novel pose scenarios. Our NBAvatar achieves the best mean LPIPS (0.052), reducing perceptual distance by 21.2% over both baselines. On three out of four subjects (S1, S3, S4), NBAvatar leads across all metrics, with particularly strong LPIPS improvements on S1 (0.034 vs. 0.050/0.051) and S3 (0.032 vs. 0.042/0.045). Subject S2 proves challenging for our method, as the parametric model fitting for this subject contains larger inaccuracies under the held-out test poses. SplattingAvatar achieves the highest PSNR on S2 (24.06 dB), which elevates its mean PSNR. Nevertheless, NBAvatar’s consistent perceptual quality advantage across the remaining subjects confirms the benefit of our hybrid representation for generalizing to unseen hand-face interaction poses.

Comparison with the InteractAvatar. We additionally report comparison with the metrics published by InteractAvatar [8] under their original evaluation protocol (Table 3). Since the evaluation code and preprocessed data used in [8] are not publicly available, we reproduced their protocol based on the description provided in the paper. Following this procedure, we crop each frame using a subject-specific bounding box covering the union of hand and face regions and resize the crop to 512×512 resolution before computing metrics. The InteractAvatar scores are taken directly from the original paper. Since their pre-

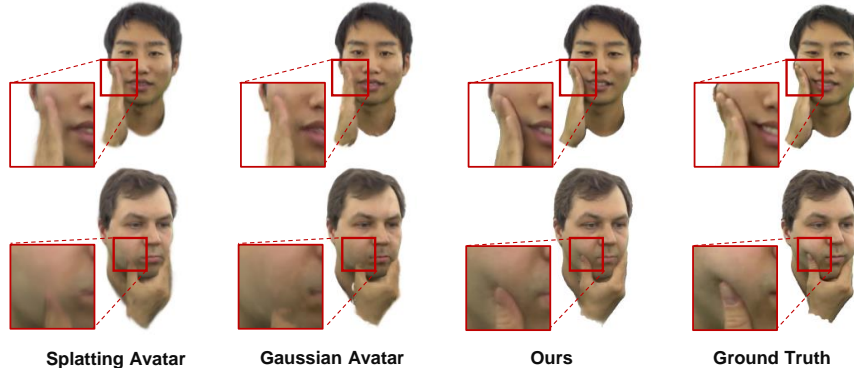


Fig. 5: Qualitative comparison on novel views. We compare our method with SplattingAvatar [46] and GaussianAvatars [40] on the Decaf [47] dataset. NBAvatar produces sharp, high-fidelity reconstructions of non-rigid facial deformations and dynamic hand appearance, accurately capturing facial details.

processed data are not publicly available, differences in implementation details may affect the comparison. We therefore encourage the reader to primarily rely on Tables 1 and 2, where all methods are evaluated under identical, fully controlled conditions.

As shown in Table 3, NBAvatar achieves the highest SSIM on both novel-view synthesis and self-reenactment tasks, indicating improved structural consistency. However, InteractAvatar reports higher PSNR and LPIPS values. We note that small differences in preprocessing and cropping can significantly affect metrics, making an exact reproduction difficult without access to the original evaluation pipeline. For this reason, we report results under a fully controlled protocol (Tables 1, 2), where all methods are evaluated using the same pipeline. Under this setting, NBAvatar consistently achieves the best objective metrics. Crucially, the qualitative comparison in Figure 4 demonstrates that NBAvatar produces visibly sharper facial details, more realistic contact deformations, and cleaner silhouettes than InteractAvatar, confirming that the quantitative gap under their protocol does not reflect the actual perceived rendering quality.

4.4 Qualitative Results

In Figure 4, we compared our results against those reported in the InteractAvatar [8] paper by retraining our approach under the same 512×512 resolution. Our NBAvatar produces fewer artifacts, especially in border regions, and yields sharper facial details. While we face PSNR and LPIPS reduction due to the inaccuracy of 3DMM fitting, our rendering results demonstrate clear quality improvement over the baseline.

Figure 5 presents a qualitative comparison on held-out novel views from the Decaf [47] dataset under megapixel resolution. Both GaussianAvatars and SplattingAvatar demonstrate Gaussian-related artifacts such as overblurred re-

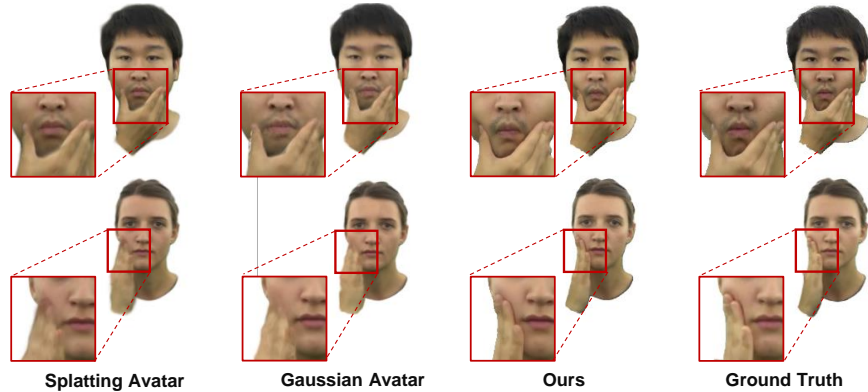


Fig. 6: Novel-pose synthesis (self-reenactment). We compare our method with SplattingAvatar [46] and GaussianAvatars [40] on held-out poses from the Decaf [47] dataset. NBAvatar generalizes to unseen hand-face interaction poses, faithfully reproducing contact-induced deformations and appearance changes.

gions and misplaced primitives caused by dynamic hand-face interaction. They are also subject to noticeable boundary artifacts where individual Gaussians protrude beyond the body silhouette. In contrast, NBAvatar produces sharp, high-fidelity reconstructions that closely match the ground truth by producing faithful shadows in hand-face interaction regions due to spatial feature aggregation in the renderer R . The combination of explicit billboard geometry with implicit neural textures enables our method to accurately capture both the geometric deformations and the appearance dynamics of hand-face interaction. Our Neural Billboard primitives, regularized to closely follow the mesh surface through our disentanglement training (Section 3.4), produce clean silhouettes free of the boundary artifacts common in Gaussian-based methods.

We further evaluate the generalization of our method to unseen poses in Figure 6. Novel-pose synthesis is particularly challenging for hand-face interaction avatars, as the model must correctly handle appearance changes for contact configurations not seen during training. Both GaussianAvatars and SplattingAvatar struggle to adapt to novel poses, especially for rendering highly-articulated hands, resulting in an increasing number of artifacts. NBAvatar maintains sharp, realistic renderings across unseen poses, demonstrating good generalisation of the proposed Neural Billboard primitives. This is achieved by the UNet renderer R learning to interpret the spatial relationships between hand and face features rather than memorizing specific training poses.

4.5 Ablation Study

We conducted an ablation study of the key components of the proposed approach in Figure 7 and report corresponding objective metrics in Table 4. Namely, we ablated the proposed segmentation \mathcal{L}_{NB} for disentanglement geometry and appearance. The exclusion of this loss results in the noise billboards' orientation,

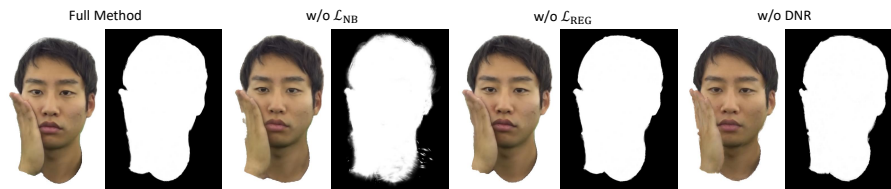


Fig. 7: Ablation study. We demonstrate renders and billboards’ masks for Subject 2 with ablated key components of the proposed algorithm.

Table 4: Ablation study on novel view synthesis for Subject 2 from Decaf dataset.

Configuration	PSNR \uparrow	SSIM \uparrow	LPIPS \downarrow
w/o \mathcal{L}_{NB}	26.75	0.9711	0.039
w/o \mathcal{L}_{Reg}	28.43	0.9748	0.033
w/o DNR	25.88	0.9655	0.045
Full Method	28.63	0.976	0.032

which leads to visual artifacts and a reduction in objective metrics. We also ablated the regularization term \mathcal{L}_{Reg} , which encourages Neural Billboards to stay aligned along the mesh and provides an additional metric improvement. Finally, we ablated the use of deferred rendering (DNR) and demonstrated that it is essential for handling hand-caused shadowing and non-rigid deformations. We conclude that all parts of the proposed approach are essential to get the best qualitative result and objective metrics.

5 Conclusion and Limitation

In this paper, we presented NBAvatar, a method for photorealistic rendering of head avatars with dynamic hand-face interaction. We introduced Neural Billboards, a hybrid representation that combines surface-aligned planar primitives with deferred neural rendering, enabling flexible geometry together with high-frequency appearance synthesis. We further proposed a geometry-aware training scheme with intermediate silhouette supervision that stabilizes the joint optimization of billboard geometry and neural texture features. Finally, we showed that spatial feature aggregation in screen space can implicitly capture complex interaction effects without explicit interaction-conditioned modules. Experiments on the Decaf dataset demonstrate improved perceptual quality and objective metrics such as PSNR, SSIM, and LPIPS under high-resolution rendering compared to Gaussian-based avatar methods. In particular, we demonstrated LPIPS reduction up to 30% compared to the baselines.

The major limitation of our method is its sensitivity to the quality of 3DMM fitting, which can affect objective metrics. In future work, we plan to investigate the possibility of adding a pose-dependent warping mechanism to enable Neural Billboards more efficiently compensate for FLAME and MANO fitting errors.

References

1. Bashirov, R., Larionov, A., Ustinova, E., Sidorenko, M., Svitov, D., Zakharkin, I., Lempitsky, V.: Morf: Mobile realistic fullbody avatars from a monocular video. In: Proceedings of the IEEE/CVF Winter Conference on Applications of Computer Vision. pp. 3545–3555 (2024)
2. Bender, J., Müller, M., Macklin, M.: Position-based simulation methods in computer graphics. In: Eurographics (tutorials). pp. 1–32 (2015)
3. Blanz, V., Basso, C., Poggio, T., Vetter, T.: Reanimating faces in images and video. In: Comput. Graph. Forum. vol. 22, pp. 641–650. Wiley Online Library (2003)
4. Blanz, V., Vetter, T.: A morphable model for the synthesis of 3d faces. In: Seminal Graphics Papers: Pushing the Boundaries, Volume 2, pp. 157–164 (2023)
5. Bühler, M.C., Meka, A., Li, G., Beeler, T., Hilliges, O.: Varitex: Variational neural face textures. In: ICCV. pp. 13890–13899 (2021)
6. Carion, N., Gustafson, L., Hu, Y.T., Debnath, S., Hu, R., Suris, D., Ryali, C., Alwala, K.V., Khedr, H., Huang, A., et al.: Sam 3: Segment anything with concepts. arXiv preprint arXiv:2511.16719 (2025)
7. Chen, A., Xu, Z., Geiger, A., Yu, J., Su, H.: Tensorf: Tensorial radiance fields. In: ECCV. pp. 333–350. Springer (2022)
8. Chen, K., Mohan, S., Theiss, J., Oprea, S., Sridhar, S., Prakash, A.: Interactavatar: Modeling hand-face interaction in photorealistic avatars with deformable gaussians. In: ICCV. pp. 10410–10420 (2025)
9. Chen, X., Wang, B., Shum, H.Y.: Hand avatar: Free-pose hand animation and rendering from monocular video. In: CVPR. pp. 8683–8693 (2023)
10. Chentanez, N., Macklin, M., Müller, M., Jeschke, S., Kim, T.Y.: Cloth and skin deformation with a triangle mesh based convolutional neural network. In: Comput. Graph. Forum. vol. 39, pp. 123–134. Wiley Online Library (2020)
11. Corona, E., Hodan, T., Vo, M., Moreno-Noguer, F., Sweeney, C., Newcombe, R., Ma, L.: Lisa: Learning implicit shape and appearance of hands. In: CVPR. pp. 20533–20543 (2022)
12. Dimond, S., Harries, R.: Face touching in monkeys, apes and man: Evolutionary origins and cerebral asymmetry. *Neuropsychologia* **22**(2), 227–233 (1984)
13. Feng, Y., Feng, H., Black, M.J., Bolkart, T.: Learning an animatable detailed 3d face model from in-the-wild images. *ACM TOG* **40**(4), 1–13 (2021)
14. Fridovich-Keil, S., Yu, A., Tancik, M., Chen, Q., Recht, B., Kanazawa, A.: Plenoxels: Radiance fields without neural networks. In: CVPR. pp. 5501–5510 (2022)
15. Gafni, G., Thies, J., Zollhofer, M., Nießner, M.: Dynamic neural radiance fields for monocular 4d facial avatar reconstruction. In: CVPR. pp. 8649–8658 (2021)
16. Gecer, B., Ploumpis, S., Kotsia, I., Zafeiriou, S.: Ganfit: Generative adversarial network fitting for high fidelity 3d face reconstruction. In: CVPR. pp. 1155–1164 (2019)
17. Grassal, P.W., Prinzler, M., Leistner, T., Rother, C., Nießner, M., Thies, J.: Neural head avatars from monocular rgb videos. In: CVPR. pp. 18653–18664 (2022)
18. Grigorev, A., Iskakov, K., Ianina, A., Bashirov, R., Zakharkin, I., Vakhitov, A., Lempitsky, V.: Stylepeople: A generative model of fullbody human avatars. In: CVPR. pp. 5151–5160 (2021)
19. Guo, Z., Zhou, W., Wang, M., Li, L., Li, H.: Handnerf: Neural radiance fields for animatable interacting hands. In: CVPR. pp. 21078–21087 (2023)
20. Guo, Z., Zhou, W., Wang, M., Li, L., Li, H.: Handnerf++: Modeling animatable interacting hands with neural radiance fields. *IEEE Transactions on Pattern Analysis and Machine Intelligence* (2025)

21. He, H., Zheng, Y., Song, J.: Capturing head avatar with hand contacts from a monocular video. In: ICCV. pp. 13099–13108 (2025)
22. Huang, B., Yu, Z., Chen, A., Geiger, A., Gao, S.: 2d gaussian splatting for geometrically accurate radiance fields. In: ACM SIGGRAPH 2024 conference papers. pp. 1–11 (2024)
23. Kalshetti, P., Chaudhuri, P.: Intrinsic hand avatar: Illumination-aware hand appearance and shape reconstruction from monocular rgb video. In: Proceedings of the IEEE/CVF Winter Conference on Applications of Computer Vision. pp. 6120–6130 (2024)
24. Kerbl, B., Kopanas, G., Leimkühler, T., Drettakis, G.: 3d gaussian splatting for real-time radiance field rendering. *ACM TOG* **42**(4), 139–1 (2023)
25. Kingma, D.P.: Adam: A method for stochastic optimization. arXiv preprint arXiv:1412.6980 (2014)
26. Kirschstein, T., Qian, S., Giebenhain, S., Walter, T., Nießner, M.: Nersemble: Multi-view radiance field reconstruction of human heads. *ACM TOG* **42**(4), 1–14 (2023)
27. Lei, J., Wang, Y., Pavlakos, G., Liu, L., Daniilidis, K.: Gart: Gaussian articulated template models. *CVPR* pp. 19876–19887 (2024)
28. Li, J., Cao, C., Schwartz, G., Khirodkar, R., Richardt, C., Simon, T., Sheikh, Y., Saito, S.: Uraavatar: Universal relightable gaussian codec avatars. In: SIGGRAPH Asia 2024 Conference Papers. pp. 1–11 (2024)
29. Li, T., Bolkart, T., Black, M.J., Li, H., Romero, J.: Learning a model of facial shape and expression from 4d scans. *ACM TOG* **36**(6), 194–1 (2017)
30. Lombardi, S., Saragih, J., Simon, T., Sheikh, Y.: Deep appearance models for face rendering. *ACM TOG* **37**(4), 1–13 (2018)
31. Mildenhall, B., Srinivasan, P.P., Tancik, M., Barron, J.T., Ramamoorthi, R., Ng, R.: Nerf: Representing scenes as neural radiance fields for view synthesis. In: *ECCV* (2020)
32. Milletari, F., Navab, N., Ahmadi, S.A.: V-net: Fully convolutional neural networks for volumetric medical image segmentation. In: 2016 fourth international conference on 3D vision (3DV). pp. 565–571. Ieee (2016)
33. Mueller, S.M., Martin, S., Grunwald, M.: Self-touch: contact durations and point of touch of spontaneous facial self-touches differ depending on cognitive and emotional load. *PLoS one* **14**(3), e0213677 (2019)
34. Müller, M., Heidelberger, B., Hennix, M., Ratcliff, J.: Position based dynamics. *Journal of Visual Communication and Image Representation* **18**(2), 109–118 (2007)
35. Müller, T., Evans, A., Schied, C., Keller, A.: Instant neural graphics primitives with a multiresolution hash encoding. *ACM TOG* **41**(4), 1–15 (2022)
36. Mundra, A., Wang, J., Habermann, M., Theobalt, C., Elgharib, M., et al.: Live-hand: Real-time and photorealistic neural hand rendering. In: *ICCV*. pp. 18035–18045 (2023)
37. Paysan, P., Knothe, R., Amberg, B., Romdhani, S., Vetter, T.: A 3d face model for pose and illumination invariant face recognition. In: 2009 sixth IEEE international conference on advanced video and signal based surveillance. pp. 296–301. Ieee (2009)
38. Pokhariya, C., Shah, I.N., Xing, A., Li, Z., Chen, K., Sharma, A., Sridhar, S.: Manus: Markerless grasp capture using articulated 3d gaussians. In: *CVPR*. pp. 2197–2208 (2024)
39. Qi, C.R., Yi, L., Su, H., Guibas, L.J.: Pointnet++: Deep hierarchical feature learning on point sets in a metric space. *Advances in neural information processing systems* **30** (2017)

40. Qian, S., Kirschstein, T., Schoneveld, L., Davoli, D., Giebenhain, S., Nießner, M.: Gaussianavatars: Photorealistic head avatars with rigged 3d gaussians. In: CVPR. pp. 20299–20309 (2024)
41. Radl, L., Steiner, M., Parger, M., Weinrauch, A., Kerbl, B., Steinberger, M.: Stopthepop: Sorted gaussian splatting for view-consistent real-time rendering. ACM TOG **43**(4), 1–17 (2024)
42. Romero, J., Tzionas, D., Black, M.J.: Embodied hands: Modeling and capturing hands and bodies together. arXiv preprint arXiv:2201.02610 (2022)
43. Rong, V., Chen, J., Bahmani, S., Kutulakos, K.N., Lindell, D.B.: Gstex: Per-primitive texturing of 2d gaussian splatting for decoupled appearance and geometry modeling. In: 2025 IEEE/CVF Winter Conference on Applications of Computer Vision (WACV). pp. 3508–3518. IEEE (2025)
44. Ronneberger, O., Fischer, P., Brox, T.: U-net: Convolutional networks for biomedical image segmentation. In: International Conference on Medical image computing and computer-assisted intervention. pp. 234–241. Springer (2015)
45. Saito, S., Schwartz, G., Simon, T., Li, J., Nam, G.: Relightable gaussian codec avatars. In: CVPR. pp. 130–141 (2024)
46. Shao, Z., Wang, Z., Li, Z., Wang, D., Lin, X., Zhang, Y., Fan, M., Wang, Z.: Splattingavatar: Realistic real-time human avatars with mesh-embedded gaussian splatting. In: CVPR. pp. 1606–1616 (2024)
47. Shimada, S., Golyanik, V., Pérez, P., Theobalt, C.: Decaf: Monocular deformation capture for face and hand interactions. ACM TOG **42**(6), 1–16 (2023)
48. Sigg, C., Weyrich, T., Botsch, M., Gross, M.H.: Gpu-based ray-casting of quadratic surfaces. In: PBG@SIGGRAPH. pp. 59–65 (2006)
49. Song, Y., Lin, H., Lei, J., Liu, L., Daniilidis, K.: Hdgs: Textured 2d gaussian splatting for enhanced scene rendering. arXiv preprint arXiv:2412.01823 (2024)
50. Sun, M., Kou, D., Yuan, R., Yang, D., Zhai, P., Zhao, X., Jiang, Y., Li, X., Li, J., Zhang, L.: Physhand: A hand simulation model with physiological geometry, physical deformation, and accurate contact handling. arXiv preprint arXiv:2409.05143 (2024)
51. Svitov, D., Morerio, P., Agapito, L., Del Bue, A.: Haha: Highly articulated gaussian human avatars with textured mesh prior. In: Proceedings of the Asian Conference on Computer Vision. pp. 4051–4068 (2024)
52. Svitov, D., Morerio, P., Agapito, L., Del Bue, A.: Billboard splatting (bbsplat): Learnable textured primitives for novel view synthesis. In: ICCV. pp. 25029–25039 (2025)
53. Svitov, D., Morerio, P., Agapito, L., Del Bue, A.: Closeupavatar: High-fidelity animatable full-body avatars with mixture of multi-scale textures. arXiv preprint arXiv:2512.03593 (2025)
54. Thies, J., Zollhöfer, M., Nießner, M.: Deferred neural rendering: Image synthesis using neural textures. ACM TOG **38**(4), 1–12 (2019)
55. Wagner, N., Schwanecke, U., Botsch, M.: Nephim: A neural physics-based head-hand interaction model. In: Comput. Graph. Forum. p. e70045. Wiley Online Library (2025)
56. Wang, Z., Bovik, A.C., Sheikh, H.R., Simoncelli, E.P.: Image quality assessment: from error visibility to structural similarity. IEEE transactions on image processing **13**(4), 600–612 (2004)
57. Weiss, S., Bradley, D.: Gaussian billboards: Expressive 2d gaussian splatting with textures. arXiv preprint arXiv:2412.12734 (2024)

58. Wu, Q., Dou, Z., Xu, S., Shimada, S., Wang, C., Yu, Z., Liu, Y., Lin, C., Cao, Z., Komura, T., et al.: Dice: End-to-end deformation capture of hand-face interactions from a single image. arXiv preprint arXiv:2406.17988 (2024)
59. Xu, R., Chen, W., Wang, J., Liu, Y., Wang, P., Gao, L., Xin, S., Komura, T., Li, X., Wang, W.: Supergaussians: Enhancing gaussian splatting using primitives with spatially varying colors. arXiv preprint arXiv:2411.18966 (2024)
60. Xu, Y., Wang, L., Zhao, X., Zhang, H., Liu, Y.: Avatarmav: Fast 3d head avatar reconstruction using motion-aware neural voxels. In: ACM SIGGRAPH 2023 Conference Proceedings. pp. 1–10 (2023)
61. Zhang, R., Isola, P., Efros, A.A., Shechtman, E., Wang, O.: The unreasonable effectiveness of deep features as a perceptual metric. In: CVPR. pp. 586–595 (2018)
62. Zheng, Y., Abrevaya, V.F., Bühler, M.C., Chen, X., Black, M.J., Hilliges, O.: Im avatar: Implicit morphable head avatars from videos. In: CVPR. pp. 13545–13555 (2022)
63. Zheng, Y., Yifan, W., Wetzstein, G., Black, M.J., Hilliges, O.: Pointavatar: Deformable point-based head avatars from videos. In: CVPR. pp. 21057–21067 (2023)
64. Zielonka, W., Bolkart, T., Thies, J.: Instant volumetric head avatars. In: CVPR. pp. 4574–4584 (2023)

Supplementary materials for "NBAvatar: Neural Billboards Avatars with Realistic Hand-Face Interaction"

A Implementation Details

A.1 Training Details

Optimization details. All trainable parameters are optimized using the Adam optimizer with default momentum parameters ($\beta_1 = 0.9, \beta_2 = 0.999$). The renderer network R is trained with a learning rate of 1×10^{-3} . Billboard color parameters are optimized with a learning rate of 2.5×10^{-3} , while billboard rotations and scales use learning rates of 1×10^{-3} and 5×10^{-3} , respectively. The neural texture parameters are optimized with learning rates of 5×10^{-4} for both the feature texture T_i^{NT} and the opacity texture T_i^α . Billboard position offsets μ_i are optimized with a learning rate of 1.6×10^{-4} , and their learning rate is exponentially decayed during training with factor $\gamma = 0.01^{1/N}$, where N denotes the total number of optimization steps (corresponding to 35 epochs).

Spectral initialization. To stabilize the optimization of neural billboard textures, we initialize the feature textures using spectral coordinates derived from the underlying mesh geometry. Specifically, we construct the cotangent Laplacian of the mesh and extract several of its lowest-frequency eigenvectors, which form a smooth spectral basis over the surface. Intuitively, these eigenvectors act as globally consistent coordinate functions that vary smoothly across the mesh geometry. We use these spectral coordinates as initial feature channels for the billboard textures, providing a structured low-frequency embedding of the surface that helps the renderer converge to meaningful spatial representations and gradually learn high-frequency appearance details.

Train-Test camera split. Following the evaluation protocol used for the Decaf dataset in InteractAvatar, we train the avatars using seven camera views and reserve one camera for novel-view evaluation. The exact train-test camera splits used for each subject are provided in Table 5.

Table 5: Cameras setup. We used the following train-test camera split for the Decaf dataset for each subject.

Subject	Training Cameras	Evaluation Cameras
S1	110, 100, 108, 084, 111, 121, 122	102
S2	122, 110, 102, 100, 084, 111, 121	108
S3	121, 100, 108, 122, 110, 102, 111	084
S4	108, 122, 110, 102, 100, 084, 121	111

Table 6: Inference speed evaluation. We report inference speed and corresponding FPS for different stages of the rendering pipeline. We additionally investigate the inference speed of rasterization with RGB and Neural Textures (NT).

Stage	Speed (ms)↓ FPS↑	
Rasterization - RGB	1.1	880
Rasterization - NT	1.3	750
Neural Rendering - fp32	27.7	36
Neural Rendering - fp16	18.1	55
Total (NT; fp16)	19.2	52

Renderer architecture. The neural renderer R follows a U-Net encoder-decoder architecture with skip connections between corresponding resolution levels. The encoder consists of five downsampling stages implemented using stride-2 convolutions followed by Instance Normalization and LeakyReLU activations. The decoder mirrors this structure and progressively reconstructs the image resolution. Instead of transposed convolutions, we employ bilinear upsampling followed by 3×3 convolutions to avoid checkerboard artifacts that commonly appear in deconvolution-based decoders. Skip connections concatenate encoder features with the corresponding decoder activations, allowing the renderer to preserve spatial details from the rasterized billboard feature map. The network predicts RGB color and opacity using two separate output heads followed by sigmoid activations.

B Inference efficiency

We evaluate the inference speed of the proposed pipeline by measuring the runtime of its main components, including billboard rasterization and neural rendering. As shown in Table 6, rasterization of billboard primitives is extremely efficient, taking only 1.3 ms when neural textures are used. The main computational cost comes from the neural renderer, which converts the rasterized feature maps into the final RGB output. Using half-precision inference (fp16) significantly reduces the rendering time from 27.7 ms to 18.1 ms without affecting visual quality. Overall, the full pipeline runs in 19.2 ms per frame, corresponding to 52 FPS at a resolution of 1024×1024 . This demonstrates that our method achieves real-time performance even at megapixel resolution. The renderer could be further accelerated using standard CNN optimization techniques such as pruning, knowledge distillation, or quantization.

C Visual Results

In Figure 8 and Figure 9, we provide additional visual results for more subjects under novel view and poses scenarios. NBAvatar produces a more faithful reconstruction of hand–face interactions compared to baselines. In Figure 10 we also report more examples of cross-reenactment.

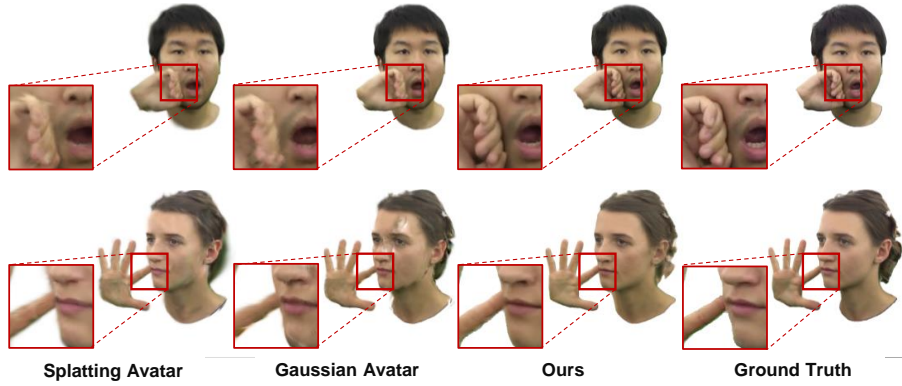


Fig. 8: Qualitative comparison on novel views for additional subjects. We compare our method with SplatingAvatar [46] and GaussianAvatars [40] on the Decaf [47] dataset. Our NBAvatar produces sharp, high-fidelity reconstructions of non-rigid facial deformations and dynamic hand appearance, accurately capturing facial details.

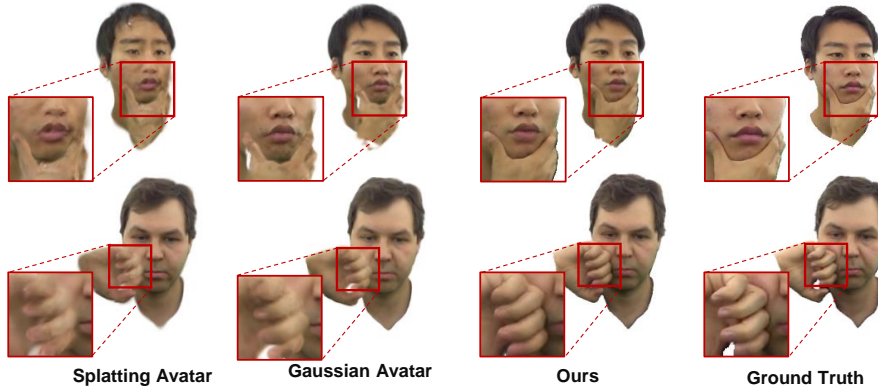


Fig. 9: Novel-pose synthesis for additional subjects. We compare our method with SplatingAvatar [46] and GaussianAvatars [40] on held-out poses from the Decaf [47] dataset. Our NBAvatar generalizes to unseen hand-face interaction poses, faithfully reproducing contact-induced deformations and appearance changes.



Fig. 10: Cross-reenactment for different subjects. We report more examples of cross-reenactment when we drive one actor with the poses of another.

Table 7: Number of channels. We analyzed the metrics and inference speed for Subject 2 from the Decaf dataset, and selected the optimal number of channels for Neural Textures.

Channels	PSNR \uparrow	SSIM \uparrow	LPIPS \downarrow	FPS \uparrow
3	27.01	0.969	0.042	35
6	28.63	0.976	0.032	34
12	28.68	0.976	0.032	33
24	27.79	0.973	0.033	11

D Number of Channels

We analyze the influence of the number of neural texture channels on rendering quality and inference speed. As shown in Table 7, increasing the number of channels from 3 to 6 significantly improves reconstruction quality, leading to higher PSNR and SSIM and lower LPIPS. Using only 3 channels limits the representation capacity of the neural textures, since the feature space must simultaneously encode RGB appearance as well as view- and pose-dependent effects such as color changes and local deformations caused by hand–face interaction. In our experiments, we increase the number of channels by doubling them at each step (3, 6, 12, 24). While increasing the channels to 12 provides only marginal improvements, further increasing the capacity to 24 channels leads to a drop in reconstruction metrics and a significant reduction in inference speed, likely due to overfitting caused by the excessive feature capacity. Based on this analysis, we select 6 channels for Neural Textures as it provides the best trade-off between rendering quality and inference efficiency.